

# Close-coupling study of rotational energy transfer in H<sub>2</sub>O collisions with He atoms

Benhui Yang\* and P. C. Stancil†

*Department of Physics and Astronomy and the Center for Simulation Physics,  
The University of Georgia, Athens, Georgia 30602, USA*

## Abstract

Quantum close-coupling scattering calculations of rotational energy transfer (RET) of rotationally excited H<sub>2</sub>O due to collisions with He are presented for collision energies between 10<sup>-6</sup> and 1000 cm<sup>-1</sup> with para-H<sub>2</sub>O initially in levels 1<sub>1,1</sub>, 2<sub>0,2</sub>, 2<sub>1,1</sub>, 2<sub>2,0</sub>, and ortho-H<sub>2</sub>O in levels 1<sub>1,0</sub>, 2<sub>1,2</sub>, 2<sub>2,1</sub>. Quenching cross sections and rate coefficients for state-to-state RET were computed on three new H<sub>2</sub>O-He potential energy surfaces (PESs). Significant differences in the collisional parameters obtained on the three PESs were found, particularly in the ultracold regime. In the thermal regime, rate coefficients calculated on each of the surfaces are generally in better agreement and comparable, but typically larger, than those obtained in a previous calculation. Unfortunately, a lack of integrated inelastic experimental data prevents determination of a preferred PES.

---

\*Electronic address: yang@physast.uga.edu

†Electronic address: stancil@physast.uga.edu

## I. INTRODUCTION

Rotationally-inelastic collisions of molecular species by atoms or molecules, so-called rotational energy transfer (RET), is an important process in a variety of astrophysical and atmospheric environments [1] and has been studied through both experimental and theoretical methods [2]. However, such studies have usually been restricted to narrow ranges of collision energy or temperature and to low-lying rotational and vibrational levels. Conversely, atmospheric or astrophysical models of molecular gas which attempt to explore departures from local thermodynamic equilibrium (LTE) situations require comprehensive arrays of molecular collision data, i.e. state-to-state cross sections and rate coefficients. While most atmospheric/synthetic spectra studies assume the gas is in LTE, i.e. that the level populations of the atoms and molecules can be described by a Boltzmann distribution, there is reason to suspect departure from LTE, so-called non-LTE (NLTE), in a variety of environments. For example, atoms and molecules in extrasolar giant planets and cool dwarf stars, such as brown dwarfs, are likely in NLTE due to a low abundance of electrons and the strong irradiation from their companion stars. In low density gas, such as interstellar clouds or star-forming regions, the molecular level populations are well known to be in NLTE. To meet the needs of astrophysical/atmospheric modeling, large-scale studies of molecular RET are needed and are now becoming feasible.

Due to the astrophysical importance of water and helium, the H<sub>2</sub>O-He collisional system has been the subject of numerous experimental [3–7] and theoretical [8–19] studies. It is also relevant to investigations of He atom scattering from water clusters [20] and spectroscopy of water clusters in He nanodroplets [21]. For numerical astrophysical models, quantitative determinations of state-to-state cross sections and rate coefficients for H<sub>2</sub>O-He collisions are crucial. However, as measurements of these quantities are difficult, numerical models often rely on cross sections and rate coefficients derived from theoretical calculations. Since the first close-coupling scattering calculations by Green [8] in 1980 using the electron gas model potential, excitation of H<sub>2</sub>O by He has been investigated in a series of increasingly more sophisticated calculations by Green and coworkers [9–14] on improved potentials.

Accurate potential energy surfaces (PESs) for the H<sub>2</sub>O-He complex are needed for reliable theoretical simulations of energy transfer in H<sub>2</sub>O-He collisions for the He interaction with water clusters. A number of PESs [9, 12, 13, 15–19] have been developed for the H<sub>2</sub>O-He

complex. In 1992, the potential calculated previously by Green *et al.* [12] using fourth-order Møller-Plesset perturbation theory (MP4) and a counterpoise correction for basis set superposition error was extended by Maluendes *et al.* [13]. Maluendes *et al.* calculated the interaction at nine additional orientations and included diffuse functions to the molecular orbital expansion basis set. The rotational excitation rate coefficients among the lowest 45 para- and ortho-levels of H<sub>2</sub>O in collisions with He atoms were then obtained by Green *et al.* [14] for temperatures between 20 and 2000 K using this improved potential.

In 2002, Hodges *et al.* [17] developed a H<sub>2</sub>O-He PES based on scaled perturbation theory calculations and calibrated the potential at the global minimum to reproduce an estimate of the complete basis set limit at the coupled-cluster with single, double, and perturbative triple substitutions CCSD(T) level of theory. This potential, referred to as SAPT-H, was used to calculate second virial coefficients at temperatures from 100 to 2000 K, which are compared with experimental values extracted from limited data for the solubility of ice in helium. The estimated uncertainties in the calculated second virial coefficients were much smaller than those of the experimental values.

Shortly after the SAPT-H potential was published, Patkowski *et al.* [18] also reported a new H<sub>2</sub>O-He PES, referred to as the SAPT-P potential, obtained with symmetry-adapted perturbation theory (SAPT) with the water molecule assumed rigid. To achieve high accuracy, the potential was obtained for the H<sub>2</sub>O-He complex using larger basis sets (159 functions of spdfg symmetry) and more grid points (242 total) than in previous PESs. The computed points were fit by an analytic function with the correct asymptotic behavior containing 56 adjustable parameters and reproducing the computed points in the well region to within 0.03 cm<sup>-1</sup>. The SAPT-P PES was also used to calculate the interaction second virial coefficient for He-H<sub>2</sub>O which agreed well with experimental data. Using the crossed molecular beam technique, Brudermann *et al.* [5] measured relative elastic and rotationally inelastic differential cross sections for He + H<sub>2</sub>O scattering at two collision energies: 66.3 and 99.0 meV. The experimental results were compared with averaged, full close-coupling calculations of state-to-state cross sections for rotational excitation based on the SAPT-P potential. The agreement with the elastic differential cross sections was excellent, while the comparison with the inelastic results, given as energy loss spectra, was not as good. Patkowski *et al.* [18] also made an extensive comparison of their potential with the SAPT-H potential [17]. For the SAPT-P potential, calculation methods were purely *ab initio* and

included fairly high level components of SAPT. On the other hand, SAPT-H was obtained with a semi-empirical SAPT approach. However, the interaction energies at characteristic points of the SAPT-H and SAPT-P potentials are in excellent agreement. The depths of the two potentials differ only by 0.5% (see Table I).

In 2003, Calderoni *et al.* [19] reported a new PES of the H<sub>2</sub>O-He complex based on coupled-cluster, Møller-Plesset, and valence bond (VB) calculations. For each computational approach, 666 non-equivalent geometrical arrangements were considered, and the PES was expressed as a linear combination of products between symmetry adapted spherical harmonics and purely radial functions. The rovibrational structure of the complex was determined under the assumption that the water molecule rotates freely, and the complex was predicted to have a single bound vibrational state and three rotational excitations. The main features of the PESs are discussed by Calderoni *et al.* and compared to the SAPT-H [17] and SAPT-P [18] potentials. In the present work, the VB potential is adopted from Ref. [19].

Parameters of the minimum of three new potentials, SAPT-H, SAPT-P, and VB, are listed in Table I, together with the parameters for the PES of Maluendes *et al.* [13]. The three new potential calculations find similar absolute minima for the H<sub>2</sub>O-He complex: a planar geometry with the He atom on the side of the O atom with a intramolecular equilibrium separation of around 5.92 a<sub>0</sub>. In spite of their resemblances in topology, the three new potentials are not fully equivalent. The depths of SAPT-H and SAPT-P are deeper than that of the VB potential. Particularly, the VB potential has the deepest isotropic term, while its main anisotropic contribution is smaller. The three new potential minima are up to 28% deeper than that of the potential of Maluendes *et al.*

More recently, Cappelletti *et al.* [6] reported a molecular-beam study of the H<sub>2</sub>O-He system including total and differential elastic cross section measurements. Cappelletti *et al.* also calculated the total integral elastic cross section using isotropic potentials obtained by spherical averages of the SAPT-H, SAPT-P and VB PESs, and an isotropic Morse-spline-van der Waals (MSV) potential fitted to their measurements. None of the three new potentials could fully reproduce the experimental data, although an improvement can be seen from SAPT-H to SAPT-P to VB. Cappelletti *et al.* also calculated the elastic differential cross section at the two collision energies of the experiment using the spherically averaged SAPT-P potential and compared it with similar calculations on their fitted isotropic potential. The

comparison to their experimental results was found to be excellent.

While agreement between experimental elastic data and calculations using either the VB or SAPT-P PES range from good to excellent, the reliability of any of the new potentials for inelastic investigations is less certain. In particular, since elastic collisions probe the short-range isotropic portion of the potential, while the intermediate- to long-range anisotropic character controls the behavior of inelastic processes, benchmarking with elastic data gives no guarantee of the reliability of inelastic theoretical results. Therefore, the aim of the current paper is to compare the inelastic dynamical performances of the SAPT-H, SAPT-P, and VB potentials. To that end, we compute quenching state-to-state data for H<sub>2</sub>O collisions with He using the close-coupling method on the three new potentials. Explicit comparison can only be made with the previous theoretical results of Green *et al.* [14] due to the lack of total inelastic experimental data.

## II. RESULTS AND DISCUSSION

Water is an asymmetric top. The theory for scattering of an asymmetric top with an atom can be found elsewhere [22, 23]. The calculations presented in this paper were performed by applying close-coupling (CC) theory. The center of the coordinate system is fixed at the center of mass of H<sub>2</sub>O. The water molecule is placed in the xz plane, with oxygen on the positive half of the z-axis. The interaction then depends only on the position of the He atom which will be described in the usual polar coordinates:  $R$ ,  $\theta$  and  $\phi$ . For the scattering calculations it is convenient to expand the angle dependence of the potential in spherical harmonics as:

$$V(R, \theta, \phi) = \sum_{\lambda\mu} v_{\lambda\mu}(R)(1 + \delta_{\mu 0})^{-1}[Y_{\lambda\mu}(\theta, \phi) + (-1)^\mu Y_{\lambda-\mu}(\theta, \phi)] \quad (1)$$

Owing to the  $C_{2v}$  symmetry of water, only even values of  $\mu$  enter the expansion. In our calculations, the H<sub>2</sub>O molecule is considered to be rigid. The rotational levels of the H<sub>2</sub>O molecule are labeled by  $j_{k_{-1}, k_{+1}}$ , where  $k_{-1}$  and  $k_{+1}$  are the  $k$  quantum numbers in the prolate and oblate limits. Rotational wave functions were obtained by diagonalizing the rigid rotor Hamiltonian using rotational constants,  $I_x = 9.278 \text{ cm}^{-1}$ ,  $I_y = 27.881 \text{ cm}^{-1}$ ,  $I_z = 14.522 \text{ cm}^{-1}$ , with rotational energy levels taken from Kyrö [24].

All the CC calculations reported here were performed using the nonreactive scattering

code MOLSCAT [25]. In the present study, we adopted the three new PESs for the H<sub>2</sub>O-He complex: SAPT-H [17], SAPT-P [18], and VB [19]. In the quantum scattering calculations, the coupled-channel equations were integrated using the modified log-derivative Airy propagator of Alexander and Manolopoulos [26] with a variable step-size. The propagation was carried out to a maximum intermolecular separation of  $R = 70 \text{ \AA}$ . Calculations were performed for collision energies between  $10^{-6} \text{ cm}^{-1}$  and  $1000 \text{ cm}^{-1}$  in order to evaluate state-to-state rate constants from  $10^{-5}$  to 200 K. At each energy, a sufficient number of total angular momentum partial waves was included to ensure convergence of the cross sections. The maximum value of the total angular momentum quantum number  $J$  employed in the calculations was 60.

Because of the orientations of nuclear spins of two hydrogen atoms, H<sub>2</sub>O is found in two species, ortho-H<sub>2</sub>O and para-H<sub>2</sub>O. The ortho- and para-levels do not interconvert in nonreactive collisions and can be treated separately. In our calculations the rotational basis sets consisted of levels up to 40 for both cases. All calculations include several energetically closed channels to ensure converged cross sections.

### A. Total quenching cross sections

Calculations of the collision energy dependence of state-to-state quenching cross sections were performed for 4 initial rotational states of para-H<sub>2</sub>O,  $1_{1,1}$ ,  $2_{0,2}$ ,  $2_{1,1}$ , and  $2_{2,0}$ , and 3 initial rotational levels of ortho-H<sub>2</sub>O,  $1_{1,0}$ ,  $2_{1,2}$ , and  $2_{2,1}$ .

The state-to-state cross sections from each initial state of H<sub>2</sub>O are summed over all final states to obtain the total quenching cross sections as a function of collision energy. In Figs. 1 and 2, we compare the total quenching cross sections of para-H<sub>2</sub>O on the SAPT-H, SAPT-P, and VB PESs. Generally, the total quenching cross sections from different initial levels on different potentials have similar behavior. Each of the cross sections exhibit the threshold behavior predicted by Wigner's Law [27] at ultra-low collision energies, where only *s*-wave scattering contributes and the cross sections vary inversely with the relative velocity. In the intermediate energy region, between  $0.1$  and  $100 \text{ cm}^{-1}$ , the cross sections display scattering resonances because of the influence of the attractive region of the interaction potential, but they reveal very different structures. Interestingly, the quenching cross section computed on the VB potential in the ultralow energy limit is larger than those obtained on the SAPT-

H and SAPT-P potentials. In the ultralow energy limit, except for the case of quenching from the  $2_{1,1}$  level, where the total quenching cross sections on the SAPT-H and SAPT-P potentials are very close, the cross sections on SAPT-P are larger than those on SAPT-H. The SAPT-H and SAPT-P potentials have slightly deeper well depths (see Table I), and lead to more resonance structure as shown in Figs. 1(b) and 1(d) for quenching from levels  $2_{0,2}$  and  $2_{2,0}$ . For energies larger than  $\sim 50 \text{ cm}^{-1}$ , the cross sections are smooth and increase with increasing collision energy, typical of rotation-translation energy transfer. The cross sections on the VB potential are smaller than those on the SAPT-H and SAPT-P potentials at higher collision energies. Also, Fig. 1 indicates that the Wigner threshold behavior occurs for energies less than  $10^{-3} \text{ cm}^{-1}$ ,  $10^{-2} \text{ cm}^{-1}$ , and  $0.05 \text{ cm}^{-1}$ , for the VB, SAPT-H, and SAPT-P potentials, respectively.

For ortho- $\text{H}_2\text{O}$  scattering by He atoms from levels  $1_{1,0}$ ,  $2_{1,2}$  and  $2_{2,1}$ , it can be seen from Fig. 2 that the quenching cross sections are of a similar magnitude as those obtained for para- $\text{H}_2\text{O}$  and show similar behavior.

## B. State-to-state quenching rate coefficients

The state-to-state cross sections (not shown) were thermally averaged over the kinetic energy distribution to yield state-to-state rate coefficients of  $\text{H}_2\text{O}$  from specific initial rotational states as functions of the temperature. The quenching rate coefficients for temperatures ranging from  $10^{-5}$  to 200 K are shown in Figs. 3-9 for para- $\text{H}_2\text{O}$  and ortho- $\text{H}_2\text{O}$ . Unfortunately, we are unaware of any experimental rate coefficient data for rotational transitions in  $\text{H}_2\text{O}$  by collisions with He. Therefore, we can only compare our results with the theoretical data of Green *et al.* [14], which were calculated on the potential of Maluendes *et al.* [13].

Considering the state-to-state quenching rate coefficients shown in Figs. 3-6 for para- $\text{H}_2\text{O}$  from initial levels,  $1_{1,1}$ ,  $2_{0,2}$ ,  $2_{1,1}$ , and  $2_{2,0}$  first, it can be seen that below a temperature of about  $10^{-3}$  K, where the rate coefficients become constant, the Wigner regime has set in. Between  $\sim 10^{-3}$  and 100 K, which is the van der Waals interaction-dominated regime, the rate coefficients exhibit an oscillatory temperature dependence due to the presence of resonances. For temperatures above  $\sim 100$  K, the rate coefficients generally increase with increasing temperature with results from the three potentials generally converging, though

they show large discrepancies at low temperatures. Comparison with the rate coefficients of Green *et al.* finds generally good agreement at temperatures above 80 K, especially for the rate coefficients on the VB potential. However, the results of Green *et al.* are smaller than the present rate coefficients calculated on the three new potentials for lower temperatures with the discrepancy increasing with decreasing temperature. Exceptions to this behavior are the transitions  $2_{0,2} \rightarrow 0_{0,0}$ ,  $2_{1,1} \rightarrow 1_{1,1}$ , and  $2_{1,1} \rightarrow 0_{0,0}$ . For the transitions  $2_{0,2} \rightarrow 0_{0,0}$  and  $2_{1,1} \rightarrow 1_{1,1}$ , the rate coefficients of Green *et al.* are in good agreement with those on the SAPT-H and SAPT-P potentials, while the rate coefficients on the VB potential about one order of magnitude smaller at high temperatures. However, the bumps near 30 K in the rate coefficients on all three new potentials are absent from the results of Green *et al.*, likely due to resonances missing from scattering on the potential of Maluendes *et al.* [13].

For scattering of ortho-H<sub>2</sub>O by He, the trends noted for the cross sections are also evident in the rate coefficients. Oscillations due to resonances and a general increase in the rate coefficients above 100 K are similar. Comparisons to the work of Green *et al.* generally show good agreement with the VB potential results. An exception is the quenching transition  $2_{1,2} \rightarrow 1_{1,0}$  where the rate coefficients of Green *et al.* are close to those on the SAPT-H and SAPT-P potentials, while the rate coefficients on the VB potential are roughly a factor of two smaller at high temperatures.

Of all of the para- and ortho-H<sub>2</sub>O transitions considered in this work, the case of  $2_{1,1} \rightarrow 0_{0,0}$  quenching has a different behavior. The rate coefficients are much smaller than other transitions and increase monotonously with temperature before becoming flat at temperatures above 100 K. All other state-to-state rate coefficients go to a constant in the zero-temperature limit in accordance with the Wigner threshold law. Further, all total quenching rate coefficients, as can be deduced from the total quenching cross section figures including quenching from the  $2_{1,1}$ , will also go to a constant at ultracold temperatures. This transition appears not to obey the Wigner law. However, its small magnitude is in agreement with the close-coupling calculations of Brudermann *et al.* [5] and the fact they find no evidence of this transition in their inelastic differential energy loss measurements at 66.3 or 99 meV. Further, they also argue that their measurements indicate a preference for  $\Delta J = \Delta k_{-1} = \Delta k_{+1} = \pm 1$  transitions preserving the character of the initial state. The largest  $\Delta J = \pm 2$  transitions are found by Brudermann *et al.* to have  $\Delta J = \Delta k_{+1}$  with  $\Delta k_{-1} = 0$  which is consistent with the current calculations.

In general, the comparisons of the current rate coefficients obtained using the three new potentials with those of Green *et al.* show that the agreement is better at higher temperatures which is relevant to astrophysical situations. However, the rate coefficients obtained with the new PESs are generally larger than those computed by Green *et al.* suggesting they might be adopted for improved astrophysical modeling. The question arises as to which potential is to be preferred and could be adopted for large-scale scattering calculations. Unfortunately, the lack of relevant experimental data and the  $\sim 1.1$ - $1.8$  dispersion in the computed results at thermal energies prevents any firm conclusion. For ultracold temperatures  $\lesssim 0.1$  K, the discrepancies are far larger. This is likely related to shifting of near zero-energy resonant states which are sensitively dependent on the van der Waals well depth as found for the H<sub>2</sub>-CO complex [28].

### III. CONCLUSION

Rotational quenching of para-H<sub>2</sub>O and ortho-H<sub>2</sub>O due to He collisions has been studied using an explicit quantum mechanical close-coupling approach on the SAPT-H, SAPT-P and VB potential surfaces. Total quenching cross sections of para-H<sub>2</sub>O and ortho-H<sub>2</sub>O from different initial states show resonance structures at intermediate energies due to the van der Waals well. The quenching rate coefficients attain finite values in the limit of zero temperature in accordance with the Wigner threshold law and the resonance structure contributes significantly to the temperature dependence of the rate coefficients. The three new potentials show different dynamical performance, particularly at low temperatures mainly due to the different van der Waals well structures. At higher temperatures state-to-state rate coefficients from the three potentials generally converge and are typically larger than rate coefficients obtained on an earlier PES by Green *et al.* Unfortunately, no experimental data exist to provide a discriminant for a preferred potential.

## Acknowledgments

BHY and PCS acknowledge support from NASA grant NNG04GM59G. We thank Dr. K. Patkowski and Dr. F. Cargnoni for providing their H<sub>2</sub>O-He potential subroutines.

---

- [1] F. Bensch and E. A. Bergin, *Astrophys. J.*, 2004, **615**, 531.
- [2] D. R. Flower, *Phys. Rep.*, 1989, **174**, 1.
- [3] R. W. Bickes, Jr., G. Duquette, C. J. N van den Meijdenberg, A. M. Rulis, G. Scoles and K. M. Smith, *J. Phys. B*, 1975, **8**, 3034.
- [4] J. T. Slankas, M. Keil and A. Kuppermann, *J. Chem. Phys.*, 1979, **70**, 1482.
- [5] J. Brudermann, C. Steinbach, U. Buck, K. Patkowski and R. Moszynski, *J. Chem. Phys.*, 2002, **117**, 11166.
- [6] D. Cappelletti, V. Aquillanti, E. Cornicchi, M. M. Teixidor and F. Pirani, *J. Chem. Phys.*, 2005, **123**, 024302.
- [7] V. Aquillanti, E. Cornicchi, M. M. Teixidor, N. Saendig, F. Pirani and D. Cappelletti, *Angew. Chem. Int. Ed.*, 2005, **44**, 2356.
- [8] S. Green, *Astrophys. J. Supp. Series*, 1980, **42**, 103.
- [9] A. Palma, S. Green, D. J. DeFrees and A. D. McLean, *J. Chem. Phys.*, 1988, **89**, 1401.
- [10] A. Palma, S. Green, D. J. DeFrees and A. D. McLean, *Astrophys. J. Supp. Series*, 1988, **68**, 287.
- [11] S. Green, *Astrophys. J. Supp. Series*, 1989, **70**, 813.
- [12] S. Green, D. J. DeFrees and A. D. McLean, *J. Chem. Phys.*, 1991, **94**, 1346.
- [13] S. Maluendes, A. D. McLean and S. Green, *J. Chem. Phys.*, 1992, **96**, 8150.
- [14] S. Green, S. Maluendes and A. D. McLean, *Astrophys. J. Supp. Series*, 1993, **85**, 181.
- [15] F.-M. Tao, Z. Li and Y.-K. Pan, *Chem. Phys. Lett.*, 1996, **255**, 179.
- [16] B. Kukawska-Tarnawska, G. Chalasinski and M. M. Szczesniak, *J. Mol. Struct.*, 1993, **297**, 313.
- [17] M. P. Hodges, R. J. Wheatley and A. H. Harvey, *J. Chem. Phys.*, 2002, **116**, 1397.
- [18] K. Patkowski, T. Korona, R. Moszynski, B. Jeziorski and K. Szalewicz, *J. Mol. Struct. (Theochem.)*, 2002, **591**, 231.

- [19] G. Calderoni, F. Cargnoni and M. Raimondi, *Chem. Phys. Lett.*, 2003, **370**, 233.
- [20] J. Bruderhmann, P. Lohbrandt, U. Buck and V. Buch, *J. Chem. Phys.*, 2000, **112**, 11038.
- [21] R. Fröchtenicht, M. Kaloudis and F. Huisken, *J. Chem. Phys.*, 1996, **105**, 6128.
- [22] S. Green, *J. Chem. Phys.*, 1976, **64**, 3463.
- [23] B. J. Garrison, W. A. Lester, Jr. and W. H. Miller, *J. Chem. Phys.*, 1976, **65**, 2193.
- [24] E. Kyrö, *J. Mol. Spectrosc.*, 1981, **88**, 167.
- [25] J. M. Hutson and S. Green, MOLSCAT computer code, version 14, Collaborative Computational Project No. 6 of the Engineering and Physical Sciences Research Council (UK), 1994.
- [26] M. H. Alexander and D. E. Manolopoulos, *J. Chem. Phys.*, 1987, **86**, 2044.
- [27] E. P. Wigner, *Phys. Rev.*, 1948, **73**, 1002.
- [28] B. H. Yang, P. C. Stancil, N. Balakrishnan and R. C. Forrey, *J. Chem. Phys.*, 2006, **123**, 104304.

Table I. The minimum of the H<sub>2</sub>O-He potentials

Potential	$R(a_0)$	$\theta(^{\circ})$	$\phi(^{\circ})$	Energy (cm <sup>-1</sup> )	Ref.
Maluendes <i>et al.</i>	6.0	90	0	-27.4	[13]
SAPT-H	5.92	75	0	-34.892	[17]
SATP-P	5.90	78.3	0	-34.94	[18]
VB	5.93	74	0	-33.82	[19]

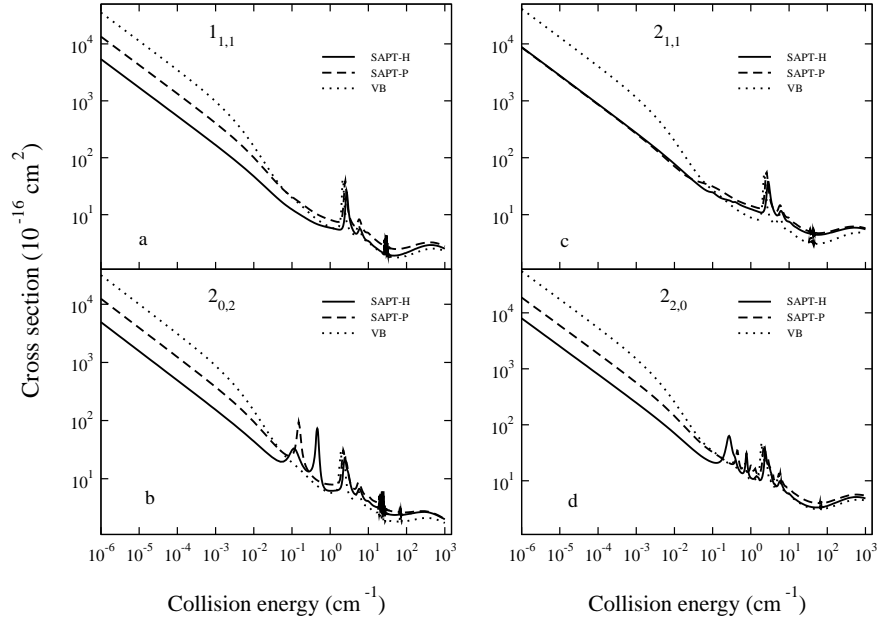


FIG. 1: Total cross sections for the quenching of para-H<sub>2</sub>O by collisions with He atoms as functions of collision energy evaluated on the SAPT-H [17], SAPT-P [18], and VB [19] potentials. Solid lines: SAPT-H; dashed lines: SAPT-P; dotted lines: VB. From initial levels: (a) 1<sub>1,1</sub>; (b) 2<sub>0,2</sub>; (c) 2<sub>1,1</sub>; (d) 2<sub>2,0</sub>.

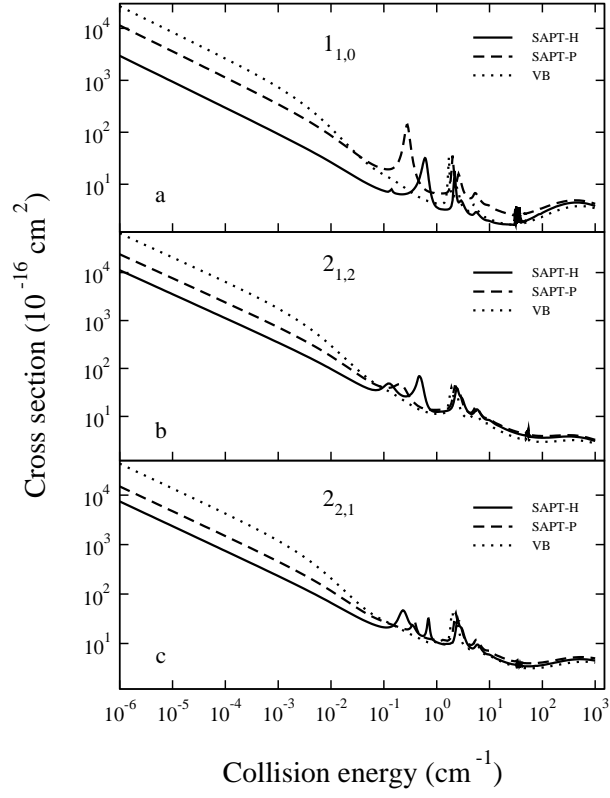


FIG. 2: Total cross sections for the quenching of ortho-H<sub>2</sub>O by collisions with He atoms as functions of collision energy evaluated on the SAPT-H [17], SAPT-P [18], and VB [19] potentials. Solid lines: SAPT-H; dashed lines: SAPT-P; dotted lines: VB. From initial levels: (a) 1<sub>1,0</sub>; (b) 2<sub>1,2</sub>; (c) 2<sub>2,1</sub>.

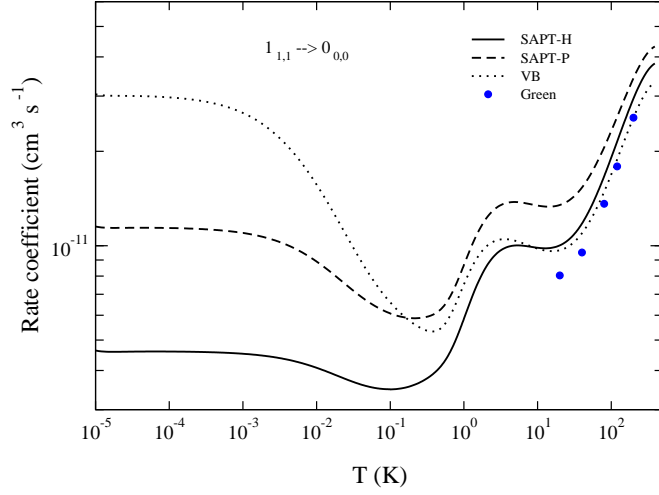


FIG. 3: Rate coefficients for the quenching  $1_{1,1} \rightarrow 0_{0,0}$ , of para- $\text{H}_2\text{O}$  in collision with He as functions of the temperature. Solid line: SAPT-H potential; dashed line: SAPT-P potential; dotted line: VB potential; solid circles: results of Green *et al.* [14].

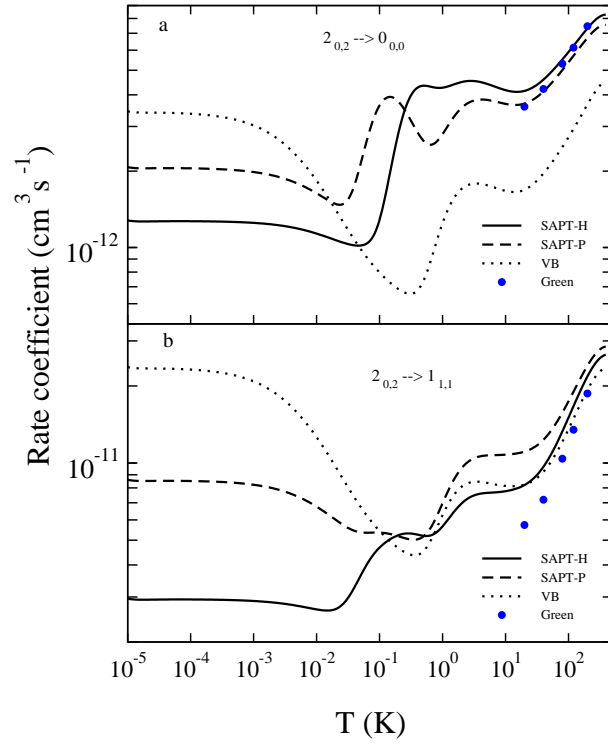


FIG. 4: Same as Fig. 3, except from initial level 2<sub>0,2</sub>. (a) 2<sub>0,2</sub> → 0<sub>0,0</sub>; (b) 2<sub>0,2</sub> → 1<sub>1,1</sub>.

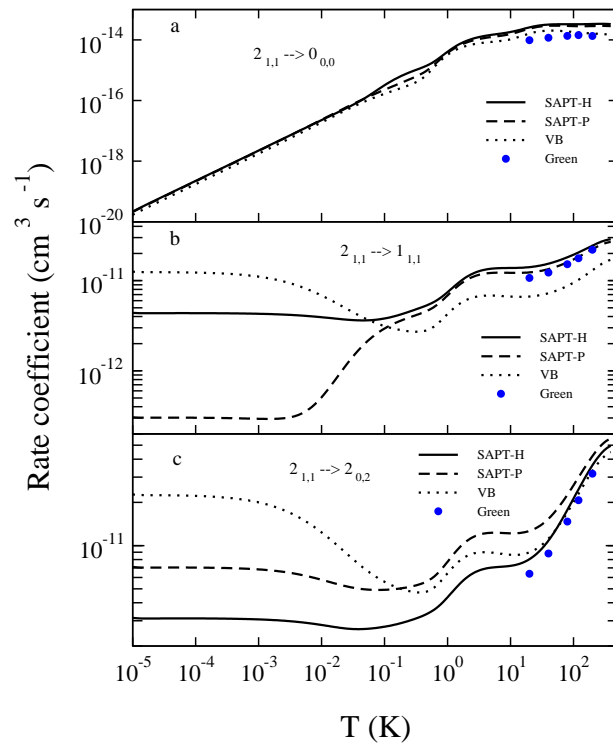


FIG. 5: Same as Fig. 3, except from initial level  $2_{1,1}$ . (a)  $2_{1,1} \rightarrow 0_{0,0}$ ; (b)  $2_{1,1} \rightarrow 1_{1,1}$ ; (c)  $2_{1,1} \rightarrow 2_{0,2}$ .

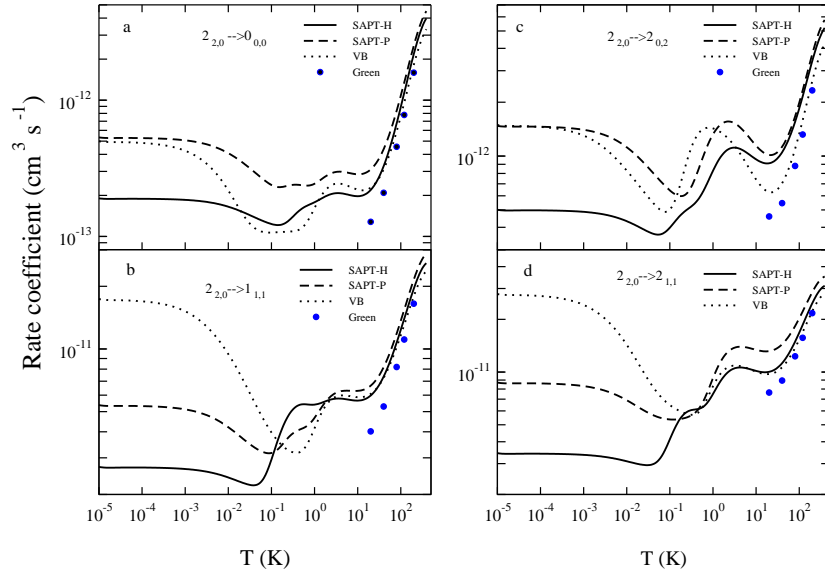


FIG. 6: Same as Fig. 3, except from initial level  $2_{2,0}$ . (a)  $2_{2,0} \rightarrow 0_{0,0}$ ; (b)  $2_{2,0} \rightarrow 1_{1,1}$ ; (c)  $2_{2,0} \rightarrow 2_{0,2}$ ; (d)  $2_{2,0} \rightarrow 2_{1,1}$ .

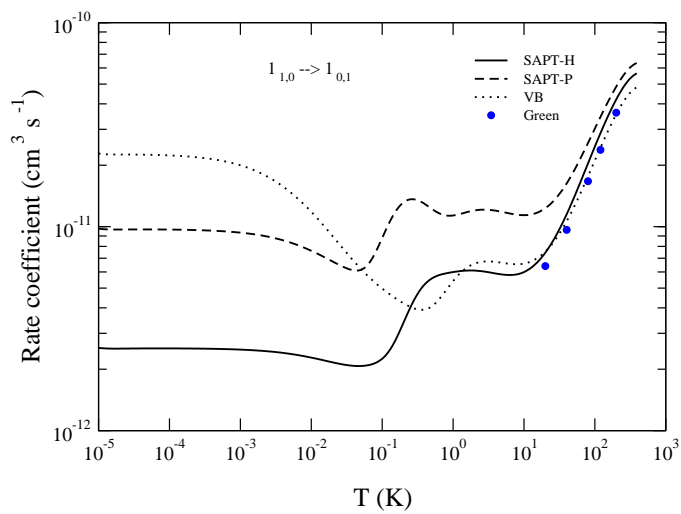


FIG. 7: Same as Fig. 3 except for quenching  $1_{1,0} \rightarrow 1_{0,1}$  of ortho- $\text{H}_2\text{O}$ .

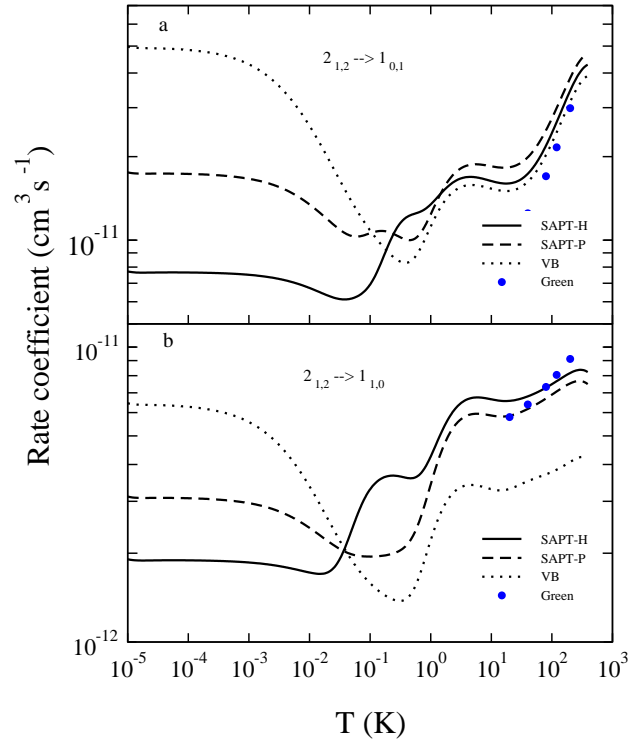


FIG. 8: Same as Fig. 7, except from initial level  $2_{1,2}$ . (a)  $2_{1,2} \rightarrow 1_{0,1}$ ; (b)  $2_{1,2} \rightarrow 1_{1,0}$ .

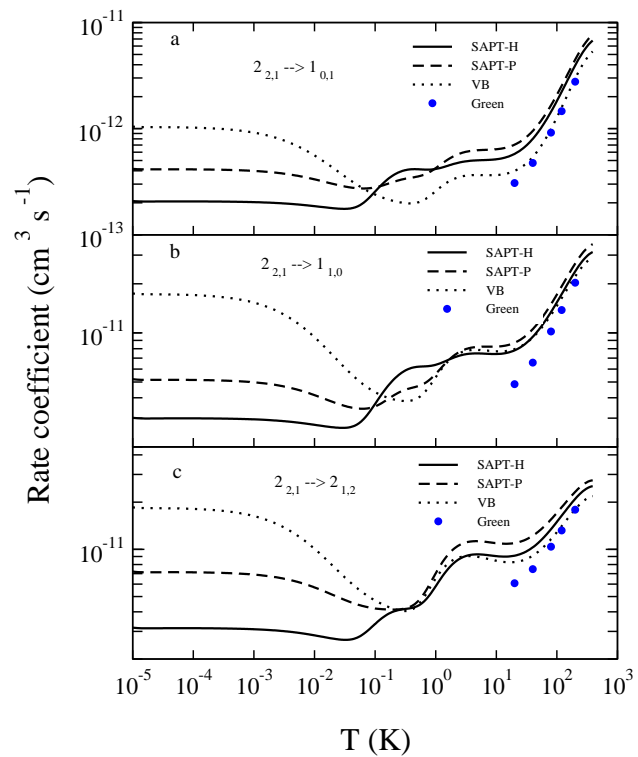


FIG. 9: Same as Fig. 7, except from initial level  $2_{2,1}$ . (a)  $2_{2,1} \rightarrow 1_{0,1}$ ; (b)  $2_{2,1} \rightarrow 1_{1,0}$ ; (c)  $2_{2,1} \rightarrow 2_{1,2}$ .